Course: Optics, Forces and Development
Santiago, Chile, January 14th - 30th, 2013

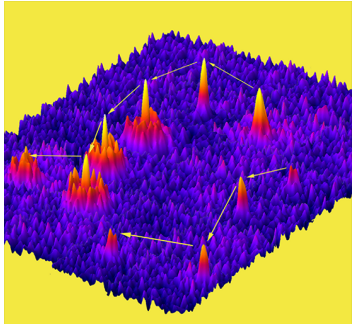

Practical aspects of confocal laser scanning microscopy

Ulrich Kubitscheck

Institute of Physical and Theoretical Chemistry
Rheinische Friedrich-Wilhelms-Universität Bonn

Contents

- Point scanning Confocal Laser Scanning Microscopy (CLSM)
- Line-scanning confocal microscopy using scanned sheet illumination
- Setups and construction
- Pros and Cons

The confocal principle

Combination of focussed laser illumination

and
detection through in pinhole placed in a conjugated optical plane

yields efficient background subtraction
and axial resolution:
„Optical Sectioning“

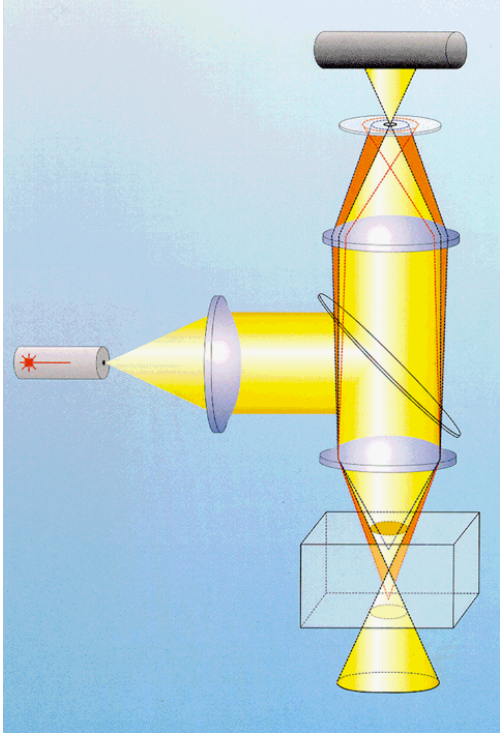

Radial and axial intensity profile of the light distribution in the focus of a lens

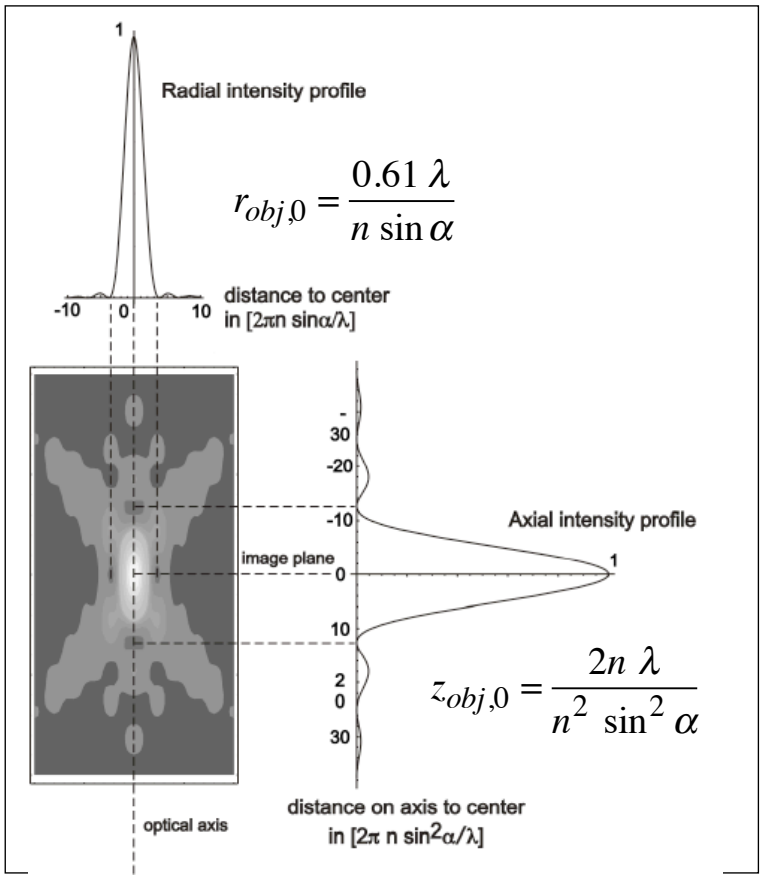

$$r_{obj,0} = \frac{0.61\,\lambda}{n\,\sin\alpha}$$

$$z_{obj,0} = \frac{2n\,\lambda}{n^2\,\sin^2\alpha}$$

Bead

Bead
normalisiert

3D representation of light focus

SPE, λ=488 nm

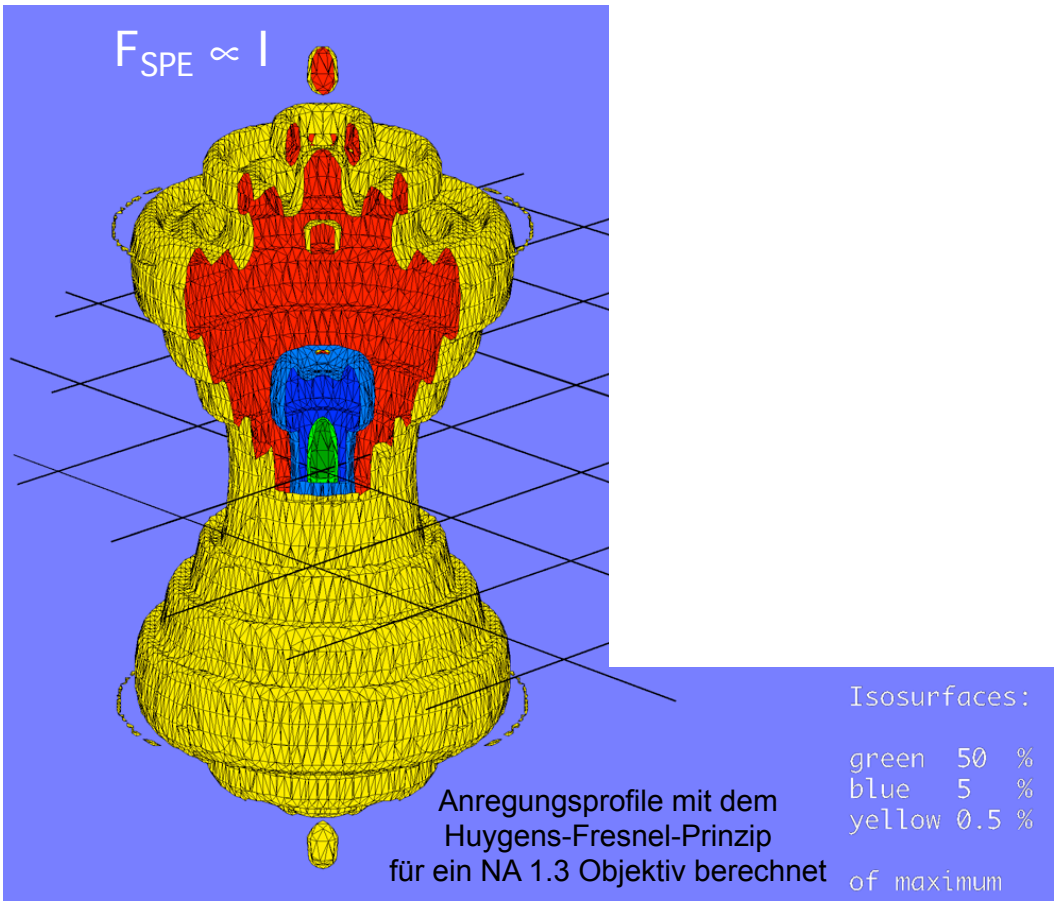

Quantitative 3D-intensity profile in the focus of an objective lens with NA = 1.3 at 488 nm

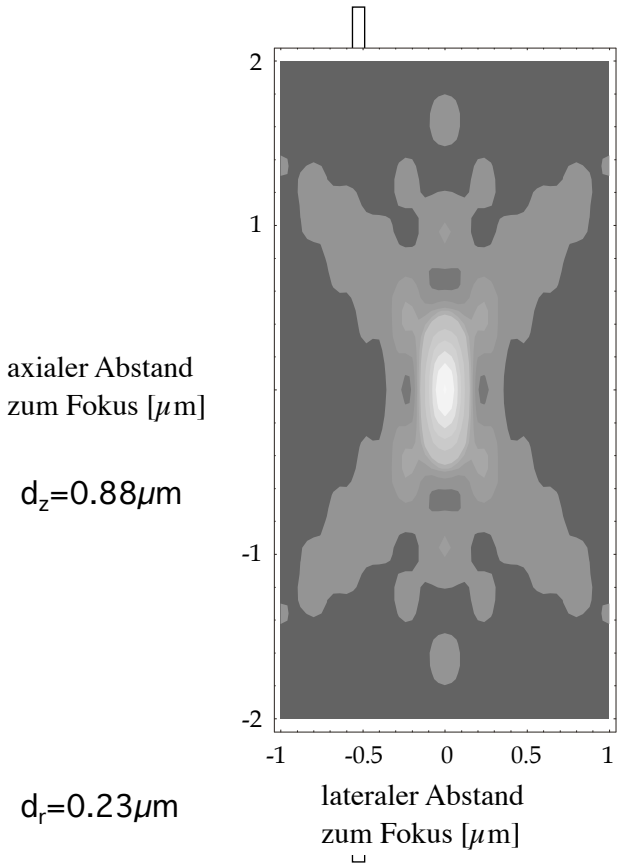

CLSM-point spread function

Excitation 488 nm Fluorescence 525 nm

axial direction

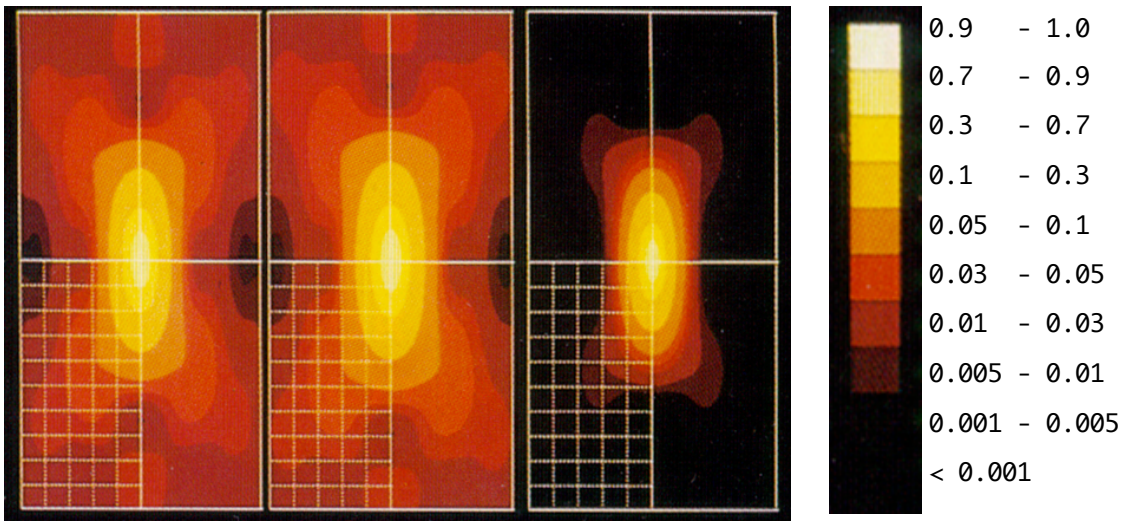

lateral direction

Objektive 100X NA 1.32
100 nm/division

Scheme of a point scanning confocal microscope

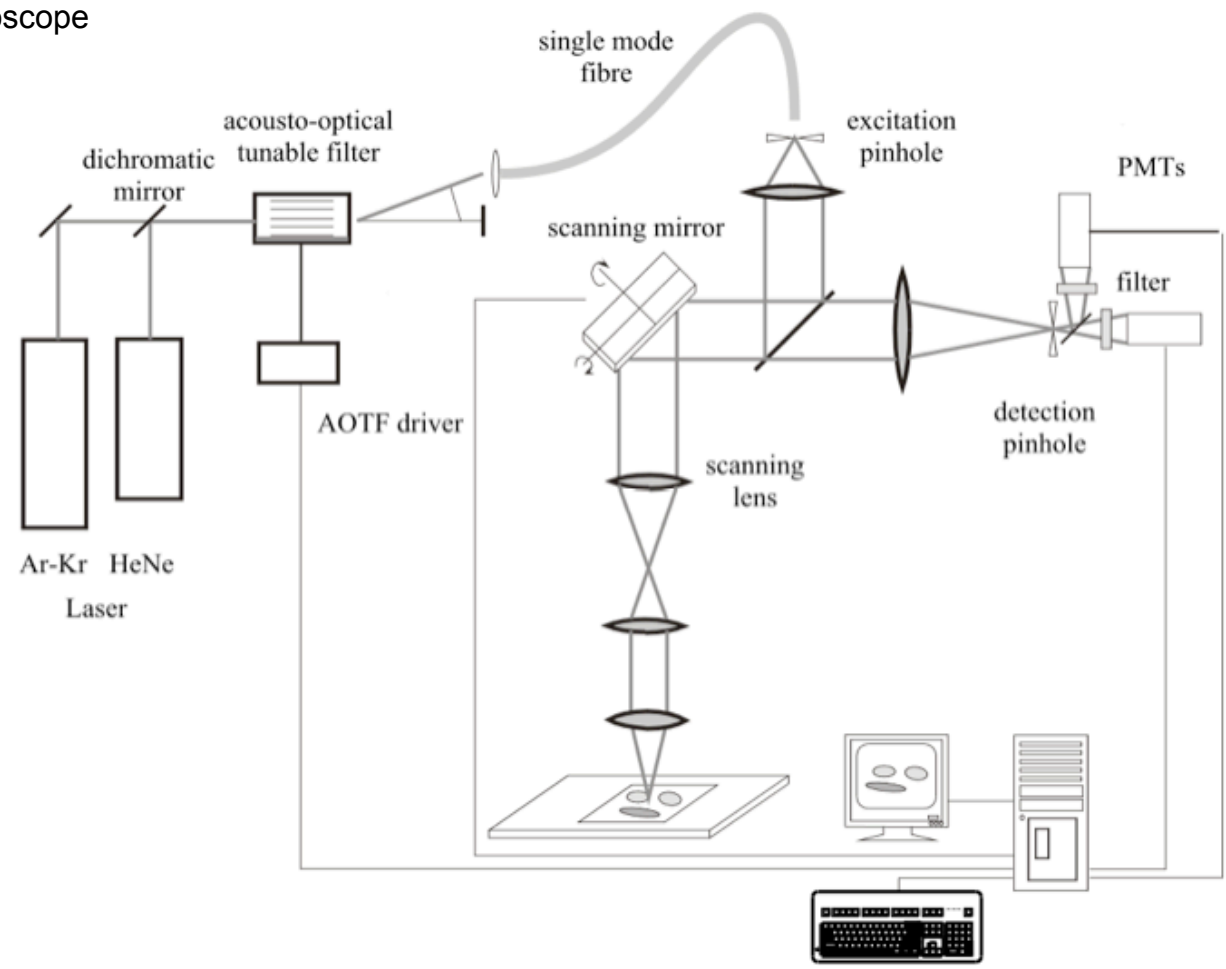

Acquisition of optical sections

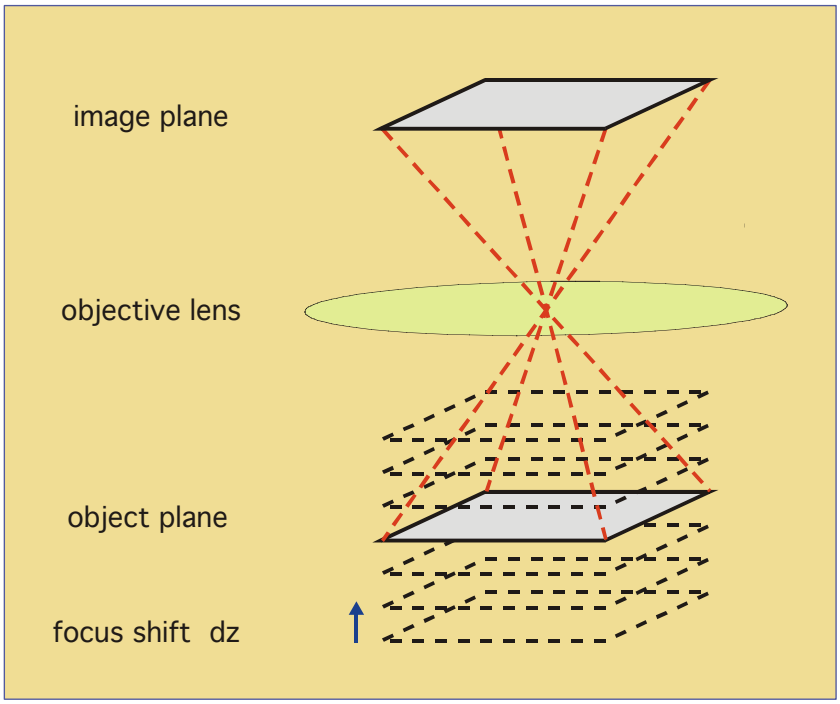

Alternatives: shift of object or shift of objective

Role of the detection pinhole

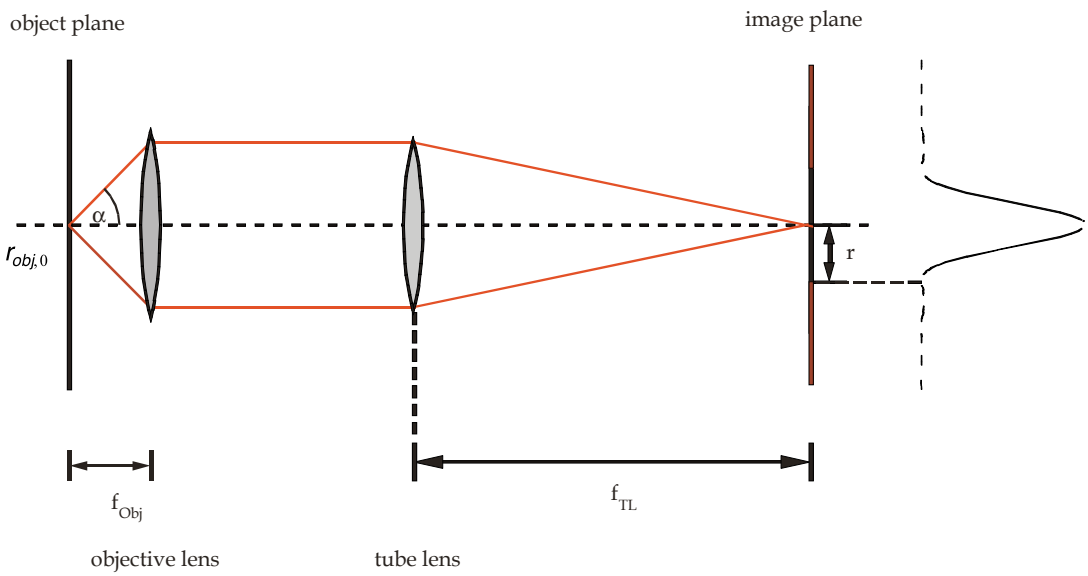

$$r_{obj,0} = \frac{0.61\,\lambda}{n \sin \alpha}$$

α: opening angle of the objective lens divided by 2
n the refractive index of the medium in front of the objective lens.

$$NA_{Obj} = n \sin \alpha$$

Detection yield, axial and lateral resolution as function of detection pinhole diameter

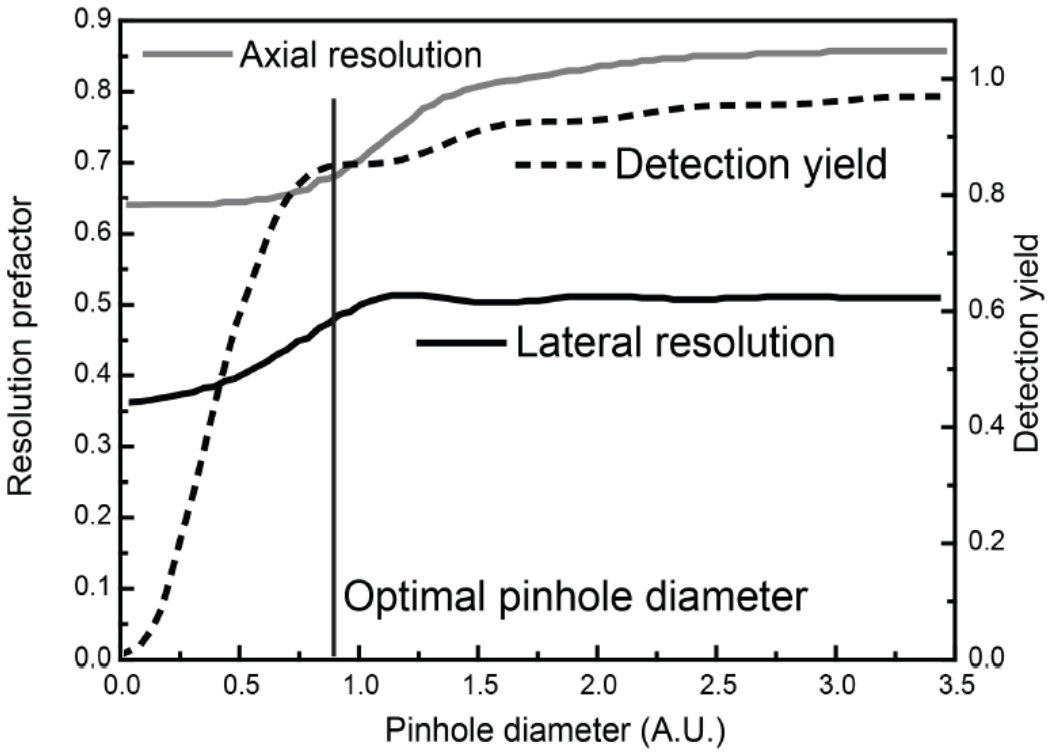

N. Naredi−Rainer, J. Prescher, A. Hartschuh, D.C. Lamb 2013, unpublished

Kinetics of a 3-state system at increasing illumination power

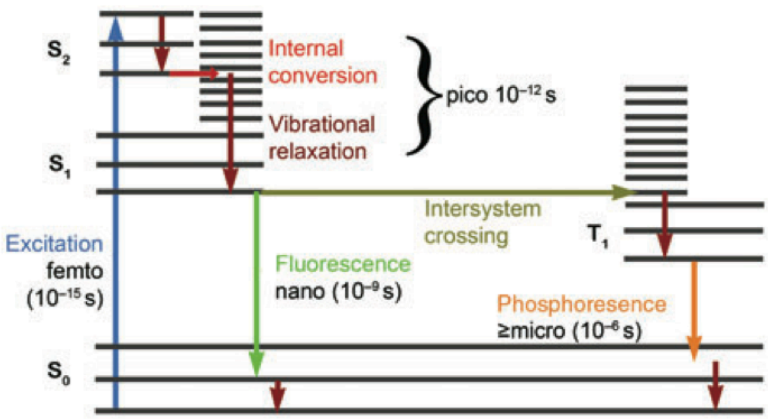

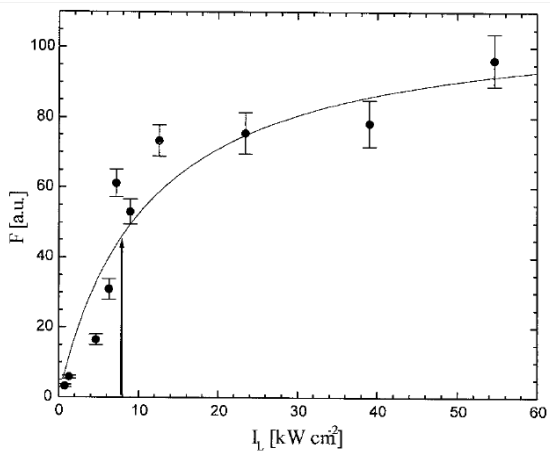

FIGURE 3 Fluorescence saturation of single GFP molecules as a function of the irradiance. Mean fluorescence intensity emitted by single GFP molecules within 10 ms was measured as a function of the incident irradiance (*symbols*). The data were fitted to Eq. 4 (*full line*), resulting in a value of 11 ± 4 kW/cm^2, at which 50% of the maximum fluorescence is emitted. *Arrow*, experimental irrradiance.

Kubitscheck et al. Biophys. J. 2000

Caveat: Fluorescence Saturation in a Point Scanning LSM

Saturation of Cy5, Alexa633 or eGFP
in aequeous solution at **2, 7** respectively **11** kW/cm^2

Maximal laser power is about 10 mW
about 10% of this at the fiber output: 1 mW
about 10% of this in the sample: 0.1 mW = 100 µW

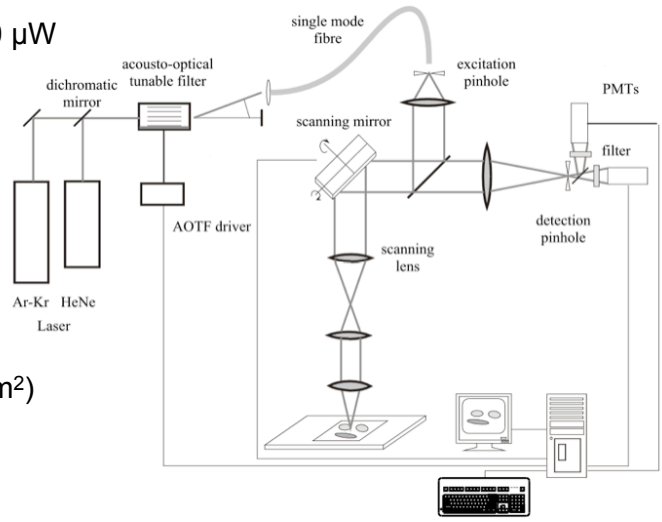

Illuminated field: ≥ diffraction limited Airy disk
of a NA1.3 objective at a wavelength of 488 nm:

$A = \pi \cdot (0.2\ \mu m)^2 \approx 0.125\ \mu m^2$

(assuming the illumination region is a circle with
a radius of 0.2 µm, see above slides 4 and 6)

Irradiation power/area:

$100\ \mu W/(0.125\ \mu m^2) = 100 \cdot 10^{-6}\ W/(0.125 \times 10^{-8}\ cm^2)$

$= 100 \cdot 10^{-6}\ W \times 8 \times 10^{8}\ /cm^2$

$= 80\ kW\ /cm^2$

Comparison

Confocal scanning microscopy	Light sheet fluorescence microscopy
High photodamage.	Reduced photo damage.
Active background rejection by pinhole.	No background excitation.
Removes also contribution from scattered light.	Scattered light is being detected → image blurred.

Comparison

Confocal scanning microscopy		Light sheet fluorescence microscopy
High photodamage.		Reduced photo damage.
Active background rejection by pinhole.	+	No background excitation.
Removes also contribution from scattered light.		Scattered light is being detected → image blurred.

Point illumination - pinhole detection
line illumination and slit detection

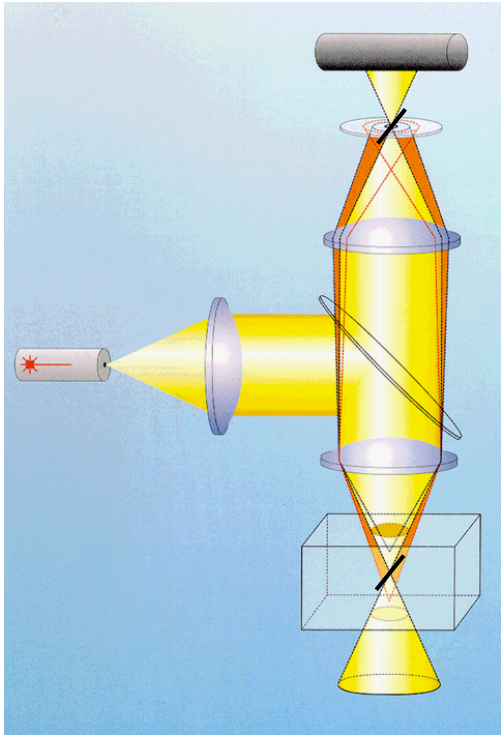

LSFM with confocal slit detection

~~High photodamage.~~		Reduced photo damage.
~~Active background rejection by pinhole.~~	+	No background excitation.
Removes also contribution from scattered light.		~~Scattered light is being detected → image blurred.~~

Scanned Light Sheet Microscopy

Philipp J. Keller, *et al.*, *Science* **322**, 1065 (2008)

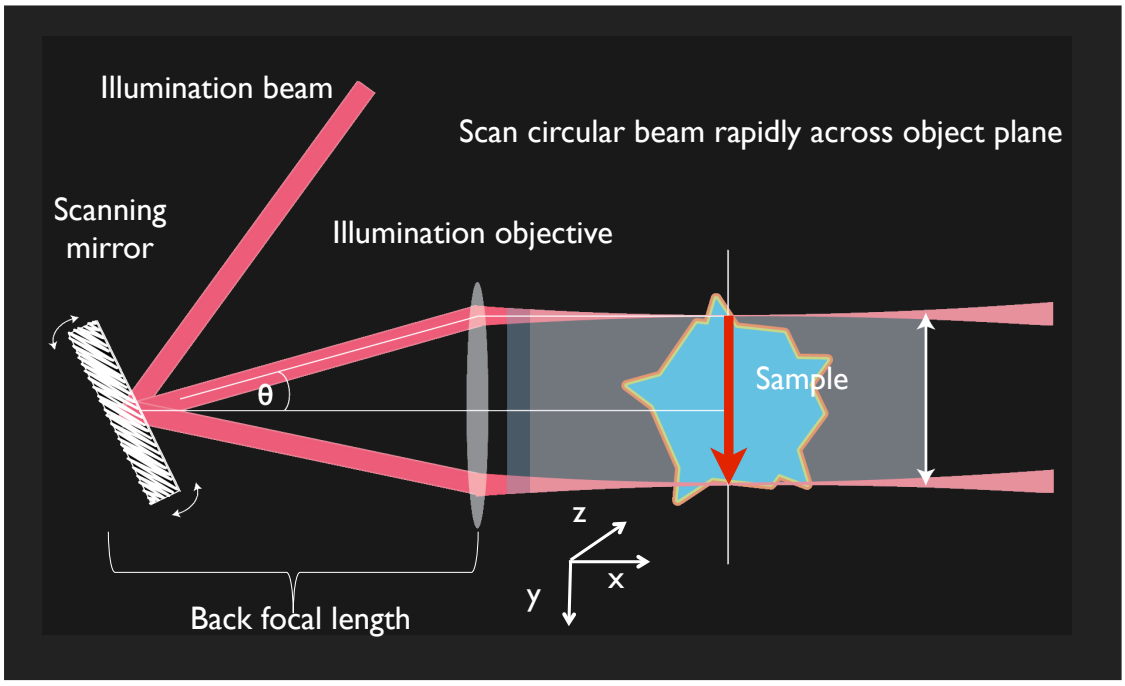

Scientific CMOS

Global shutter

1440 Px.
= 5.2 mm

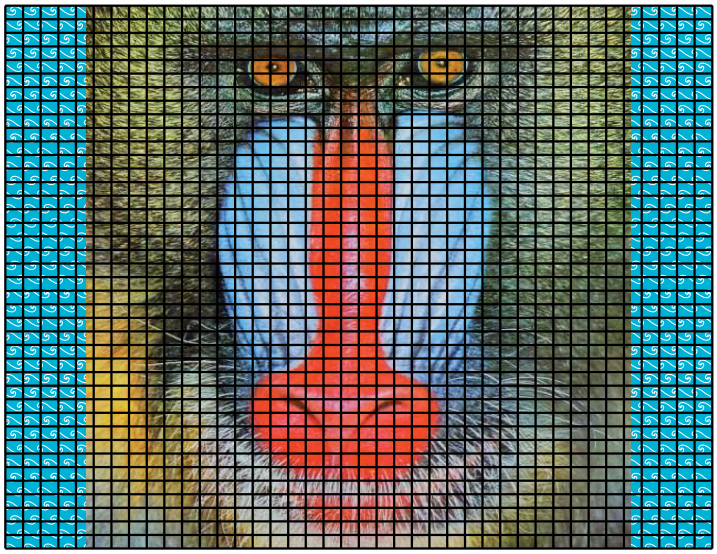

1920 Px. = 7 mm

Global shutter:
All pixel active at once.

67% QE @ 500 nm

Scientific CMOS

First line reset
and
exposure start .

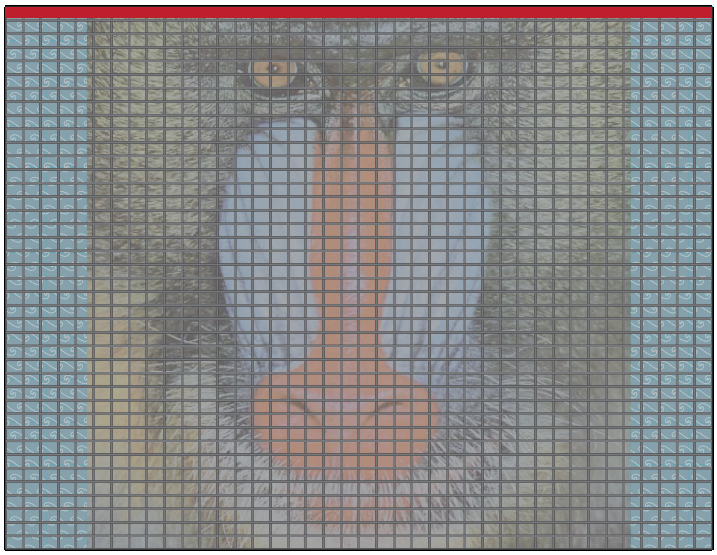

Inactive pixel rows

Scientific CMOS

Rolling shutter

Second row activated after line readout time.

Line readout time 15 µs.

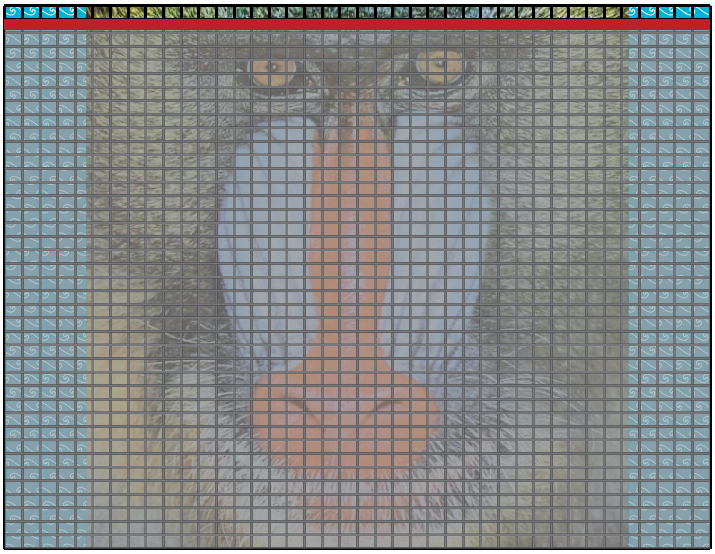

Subsequent reset and activation of pixel rows.

Scientific CMOS

Rolling shutter

Exposure stop + read-out after exposure time has passed.

Reset and exposure start.

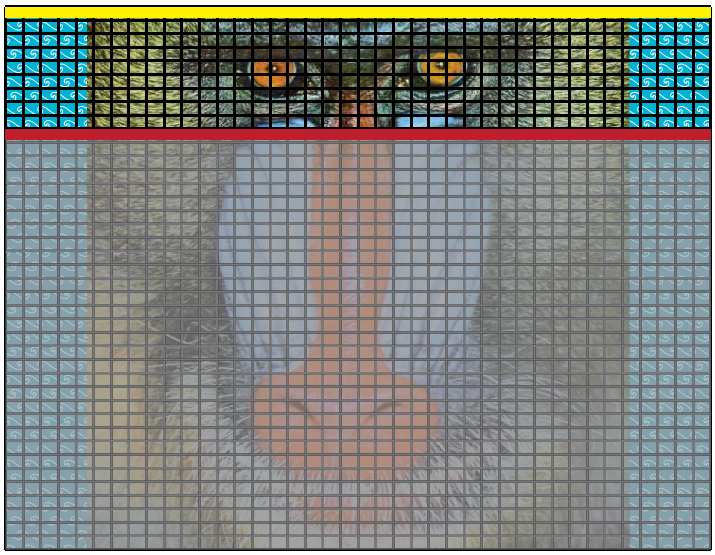

Band of simultaneous exposure.

Scientific CMOS

Rolling shutter

N active lines

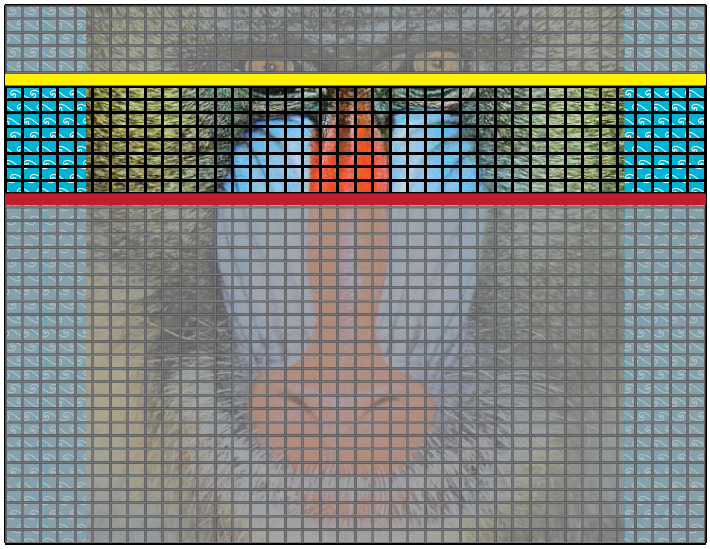

Rolling shutter mode corresponds to a vertically moving slit detector.

Width determined by exposure time.

Exposure time = N x readout time for single row

Confocal effect

H. Spiecker (LaVision BioTec), "Method and arrangement for microscopy." PCT Patent 2011/120629

Conventional configuration:

Rapidly scanned excitation

Global shutter mode

Confocal slit detection:

Narrow excitation

Slit aperture

Whole chip exposed at once

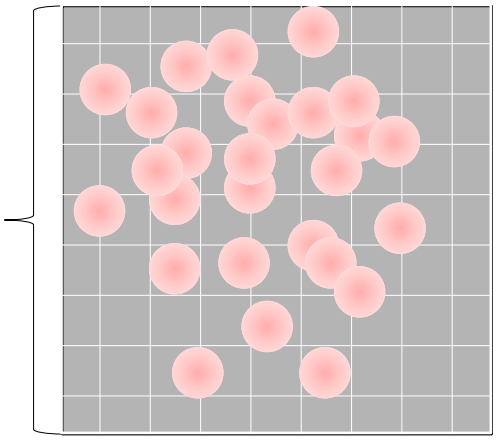

Exposed band

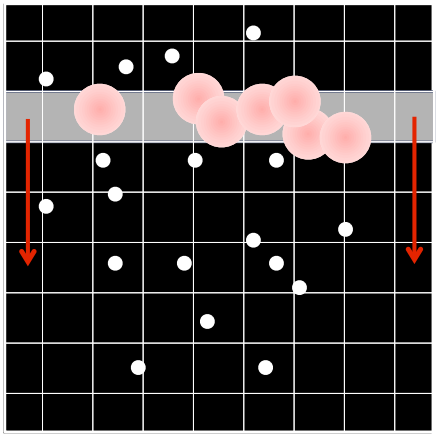

Principle of relay lenses

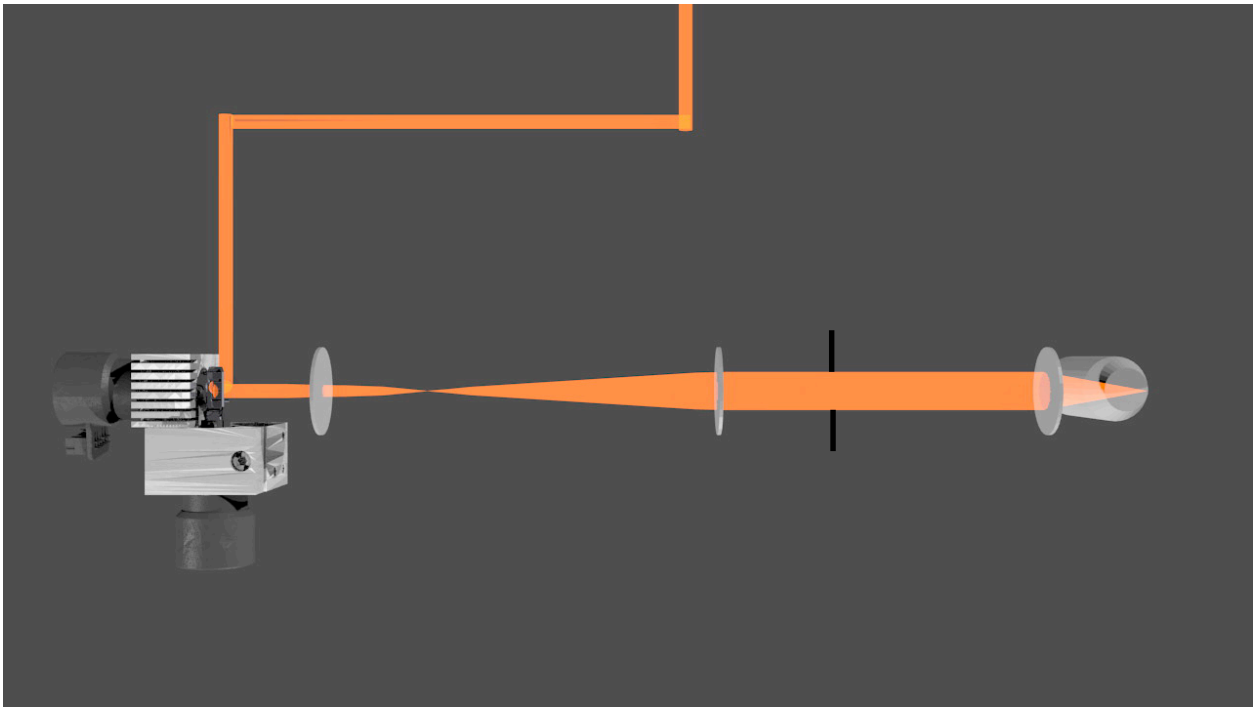

Experimental setup

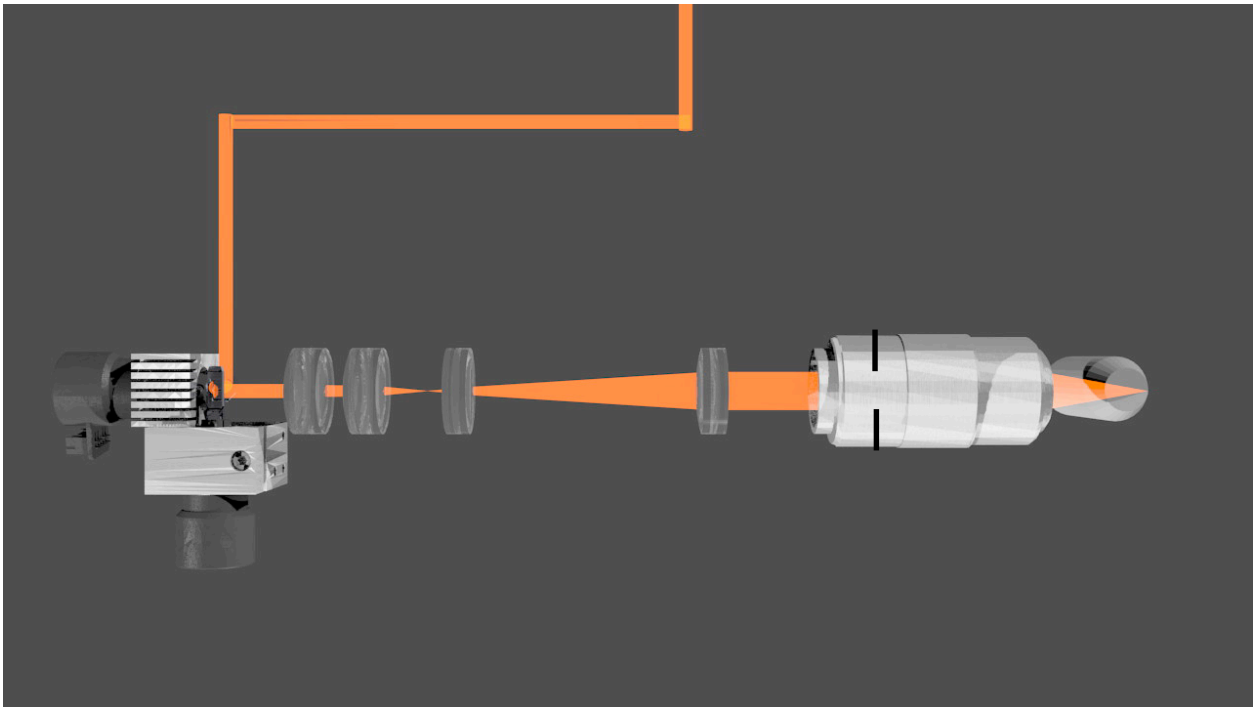

Experimental setup

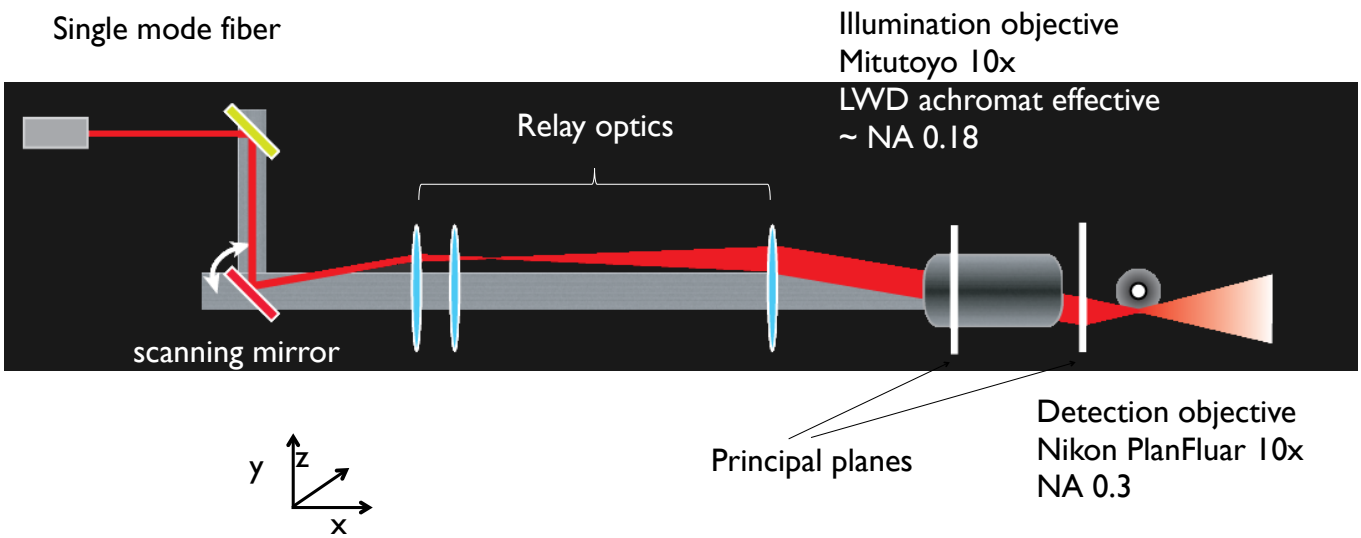

$1/e^2$ waist radius	Rayleigh length
4.4±0.1µm	138±4 µm

Scattered light suppression

Fluorescent beads (Ø 200nm) with fluorescent dye in agarose gel. λ_{exc} = 633 nm.
0,5 particles/μm^3

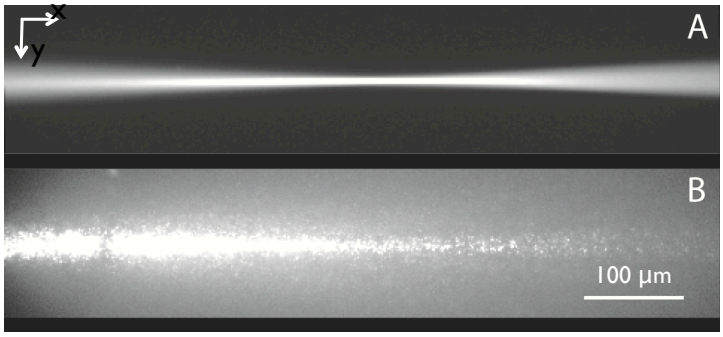

Beam in fluorescent solution.

Distorted beam in agarose with beads.

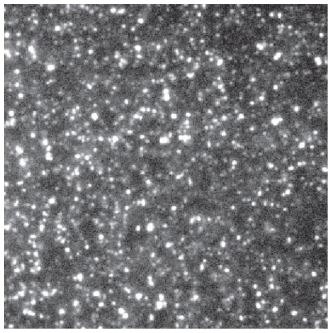

Beads imaged in global shutter mode.

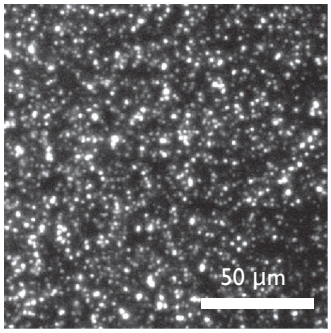

Beads imaged in rolling shutter mode.

RS width 32px/11.6µm.

Enhanced contrast and signal to noise ratio

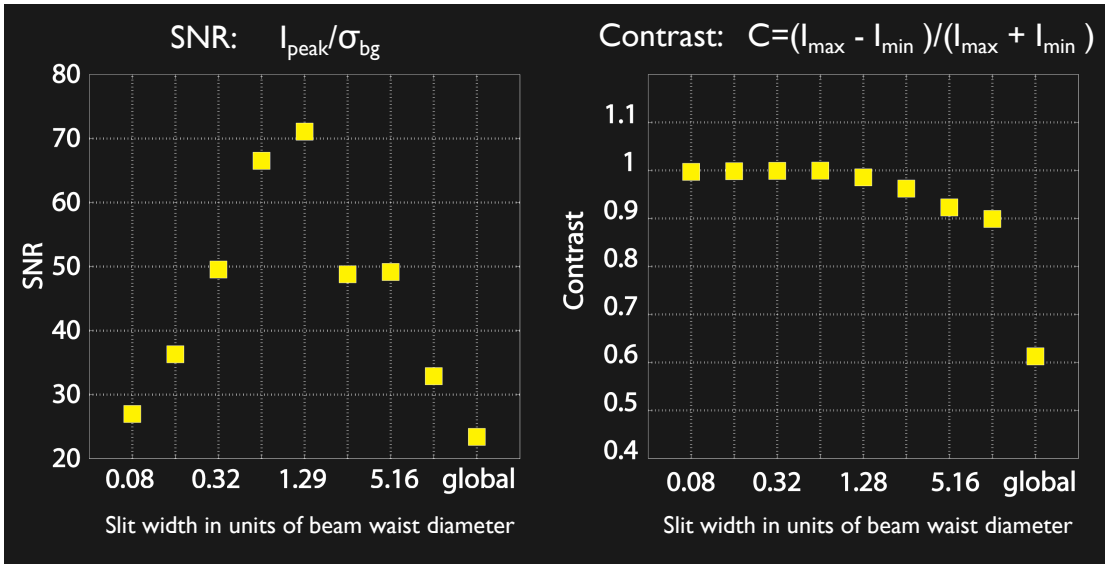

Laser intensity equal for
all measurements.

Enhanced sectioning

Global shutter mode
t_{exp} = 20 ms

Confocal slit detection,
rolling shutter 2 px, t_{exp} = 30 µs, 40x averaged

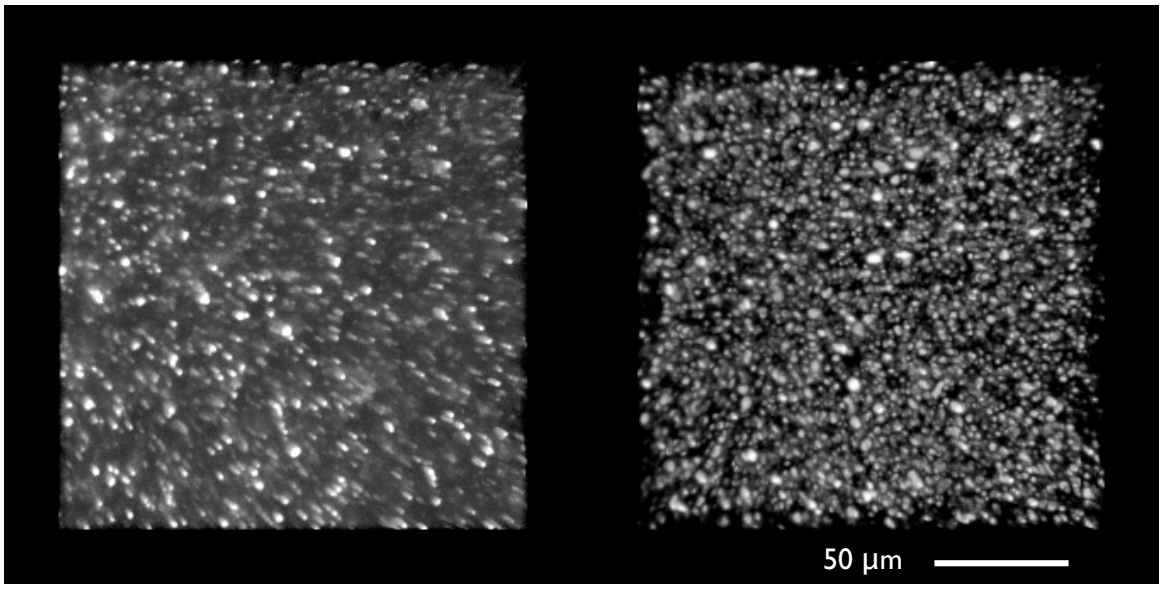

3D reconstruction from image stack. → Effective background suppression.

50 frames, 1 µm step size, 120x120x50 µm

Enhanced sectioning

Sample of fixed fluorescen beads

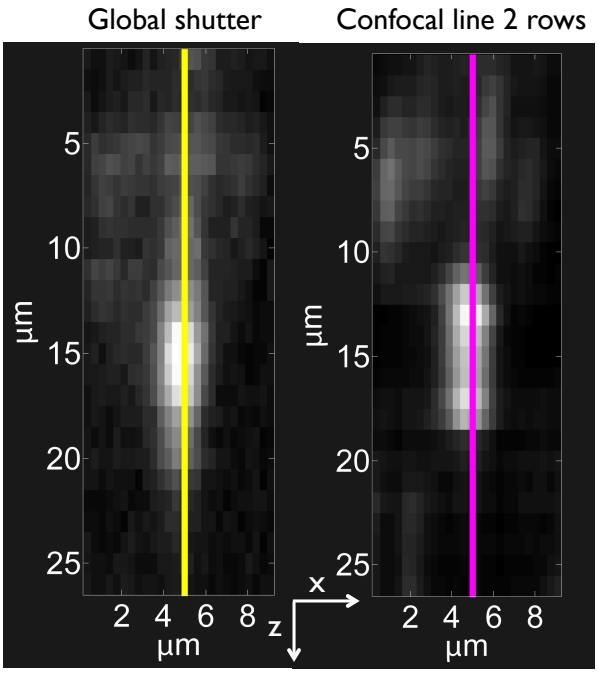

Normalized intensity

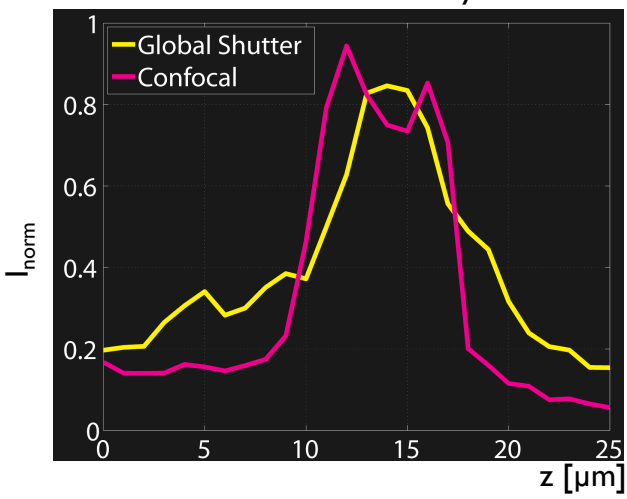

Sectioning	Global Shutter	Confocal (2 lines)
$1/e^2$ radius	4,8 ± 0,9 µm	3,8 ± 0,8 µm

Extended cleared samples

Embryonic mouse brain by courtesy of Dr. Sandra Blaess, Bonn

Acquisition of a large specimen volume: 3.13mm x 3mm x 612 µm

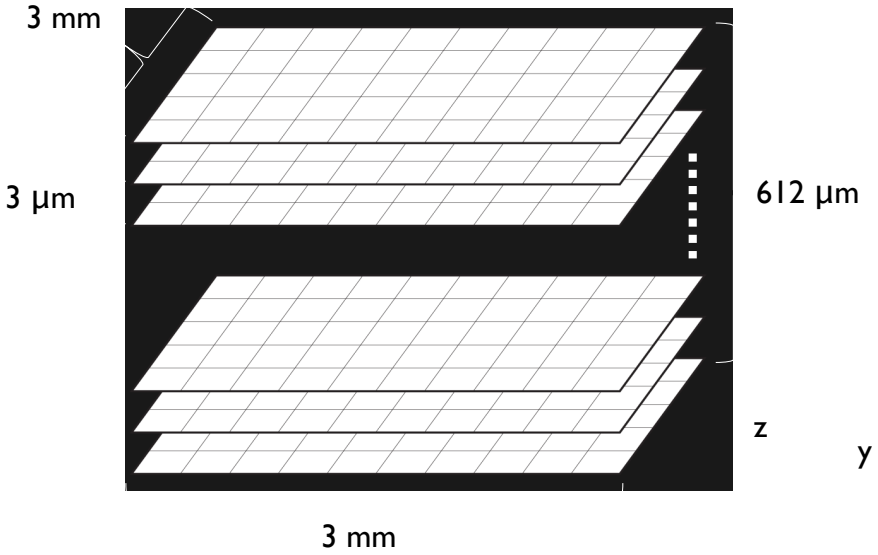

3D Mosaic
5x11 tiles per plane

Tile size:
Δx = 200µm
Δy = 600µm
Δz = 3 µm

Mouse brain 3D mosaic

Global shutter t_{exp} = 22 ms Rolling shutter t_{exp} = 0.3 ms

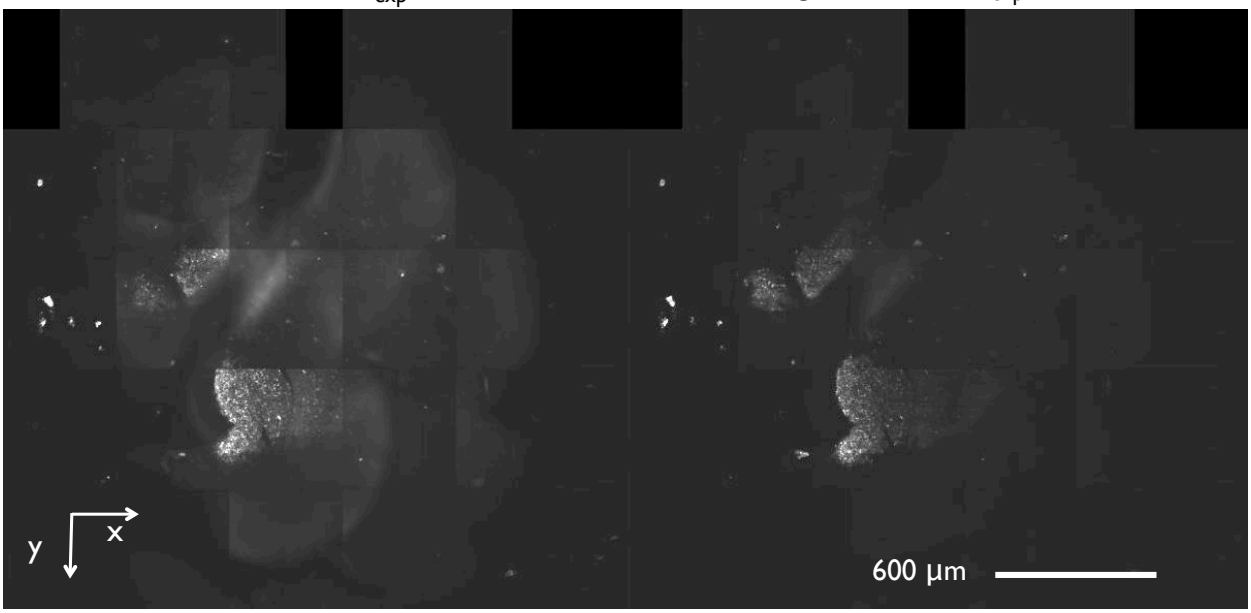

Movie starting from cover slip to 612 µm inside the sample.
Rolling shutter size = beam diameter (~9 µm). λex=532 nm.

Cell nucleus of *C. tentans* larva

Light sheet illumination of a salivary gland cell nucleus.

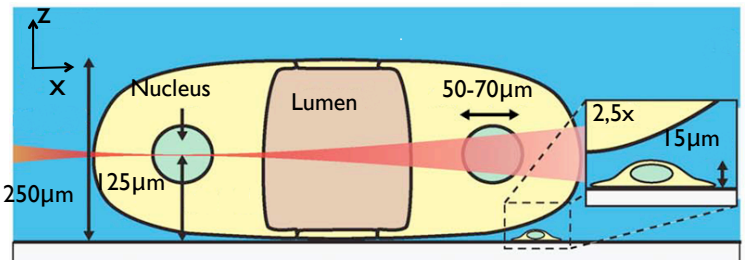

Expand illumination beam to gain better sectioning:

$1/e^2$ waist radius	Rayleigh length
2.8±0.2µm	37.6±0.6 µm

Cell nucleus of *C. tentans* larva

Global shutter t_{exp} = 20 ms Rolling shutter t_{exp} = 0.6 ms

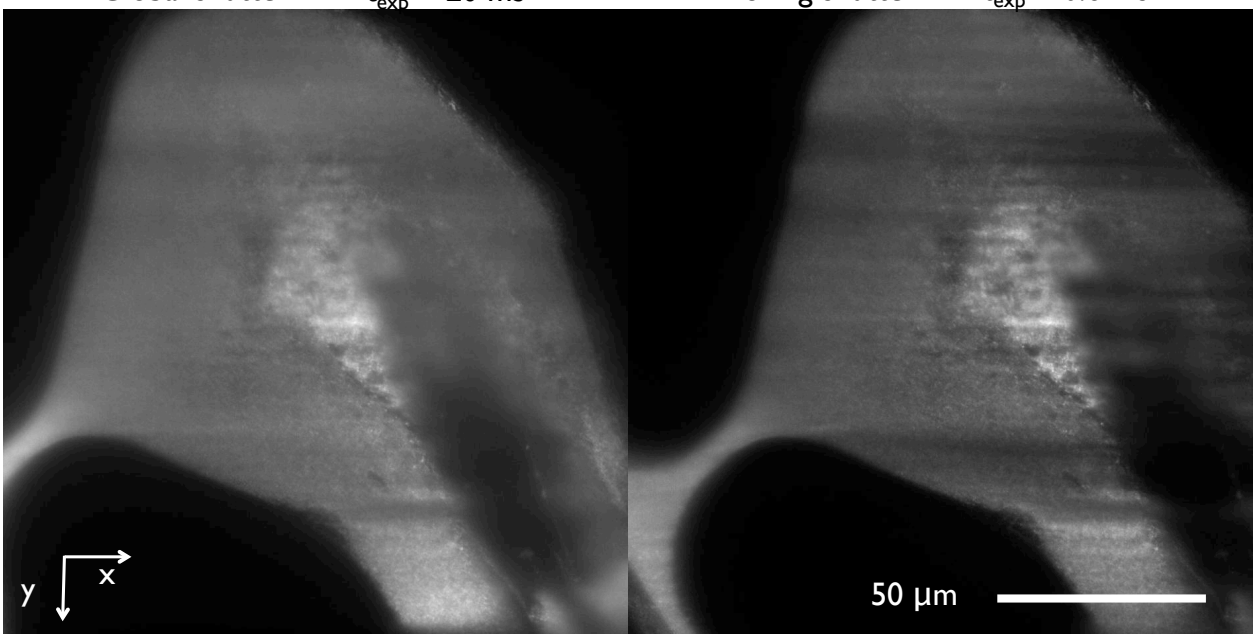

Rolling shutter size = $1/e^2$ beam diameter (~5 µm). λ_{ex}=532 nm.
Detection: Nikon objective 40X NA 1.1, W, LWD

Filtering of shadow artefacts

Global shutter Rolling shutter Rolling shutter destriped

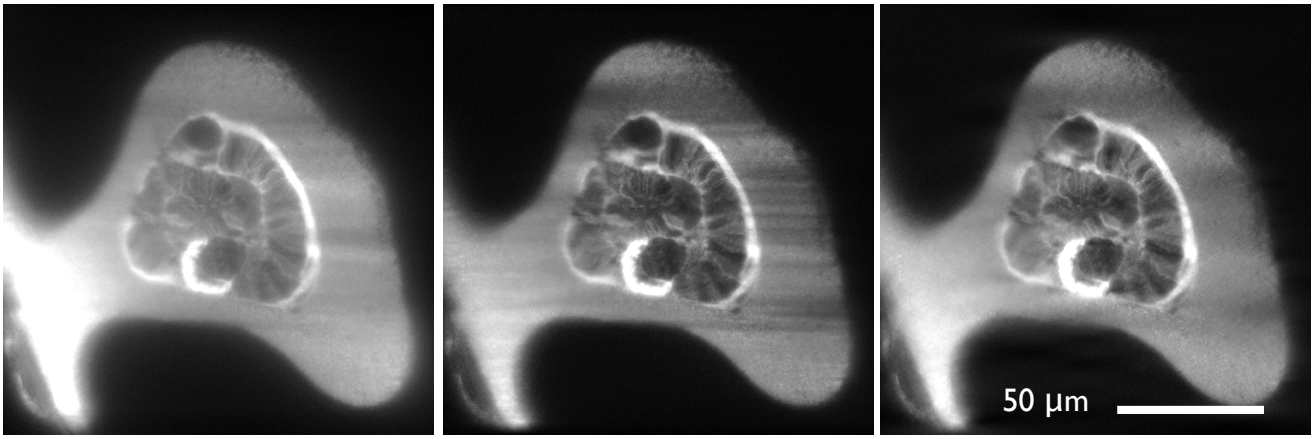

Destriping algorithm based on wavelet and Fourier filtering according to

Münch et al. 2009, Stripe and ring artifact removal with combined wavelet-Fourier filtering, Optics Express 17, 8567-91

C. tentans salivary gland cell

Contrast improvement

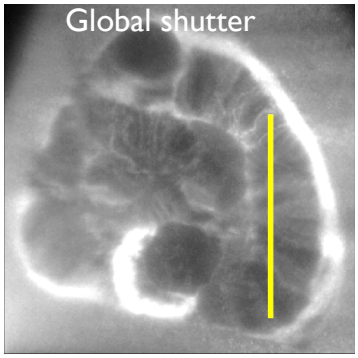

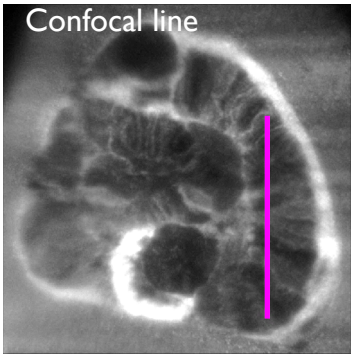

Normalized intensity along yellow, magenta and cyan line, respectively.

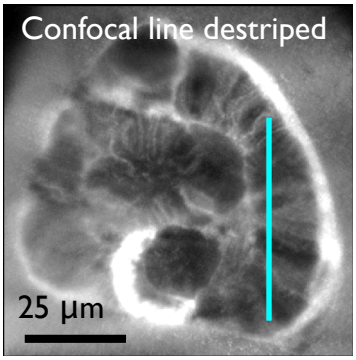

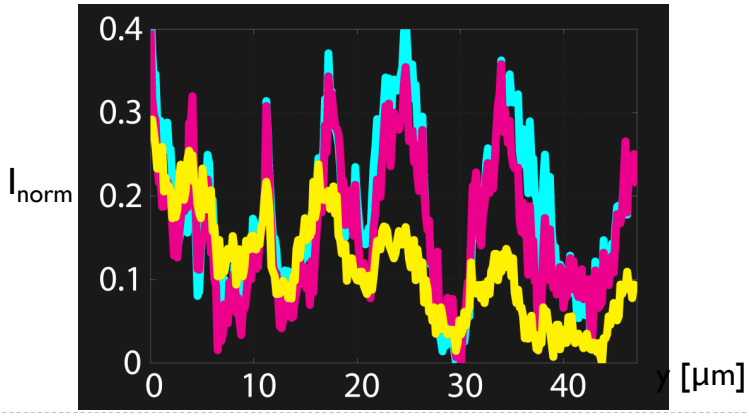

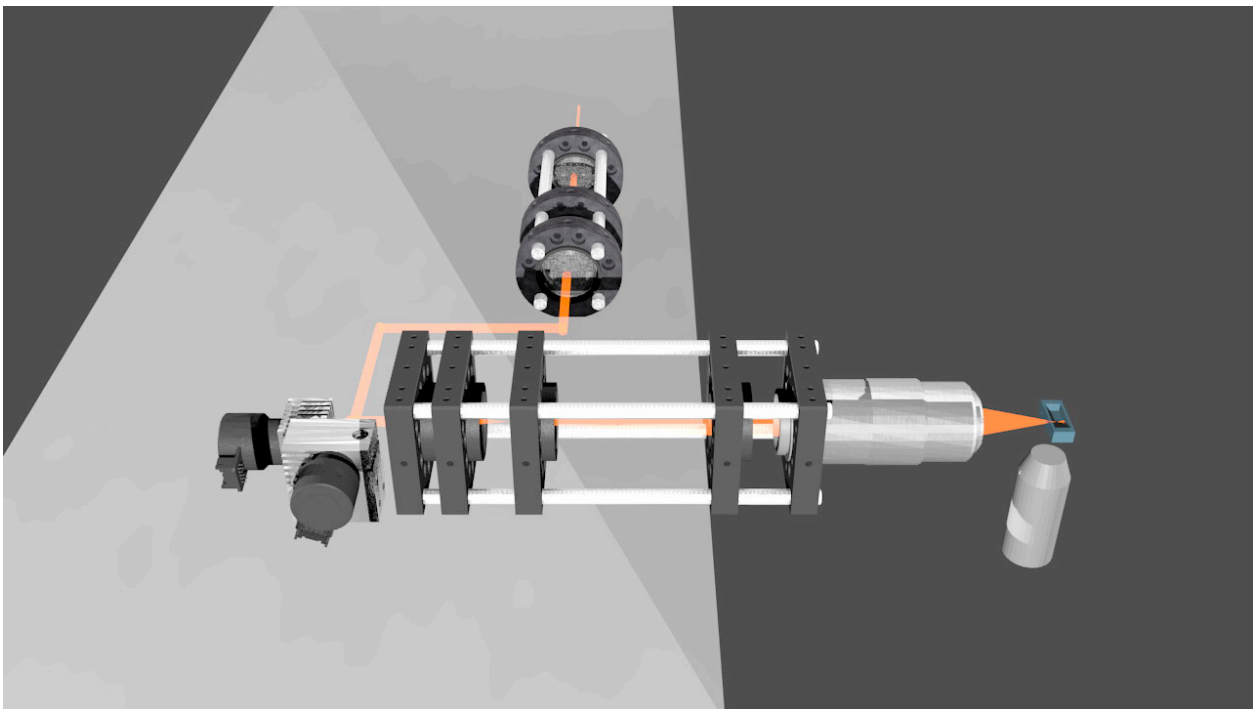

Summary

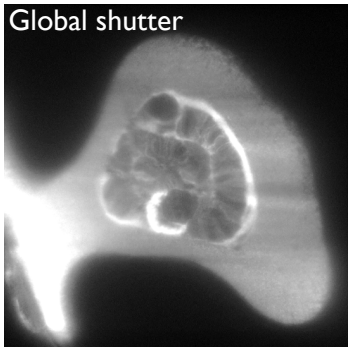

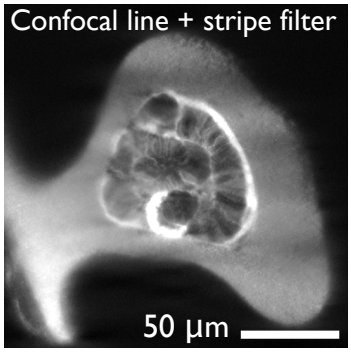

Scanned Gaussian beam synchronized with sCMOS rolling shutter.

Blocking of scattered light and elimination of background.

Improved contrast and SNR without increase of illumination intensity.

Better sectioning and increased penetration depth.

Particularly suited for imaging uncleared and living samples.

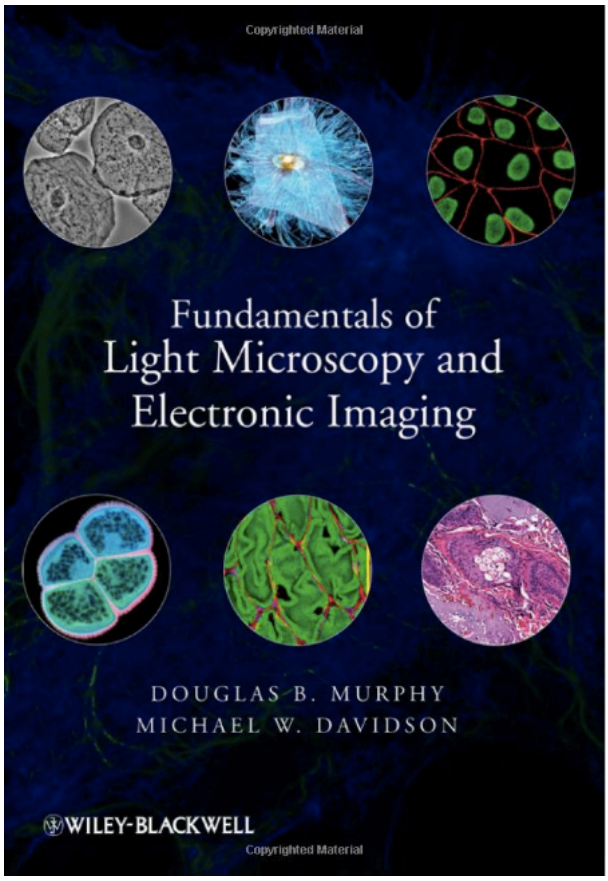

2nd edition just published

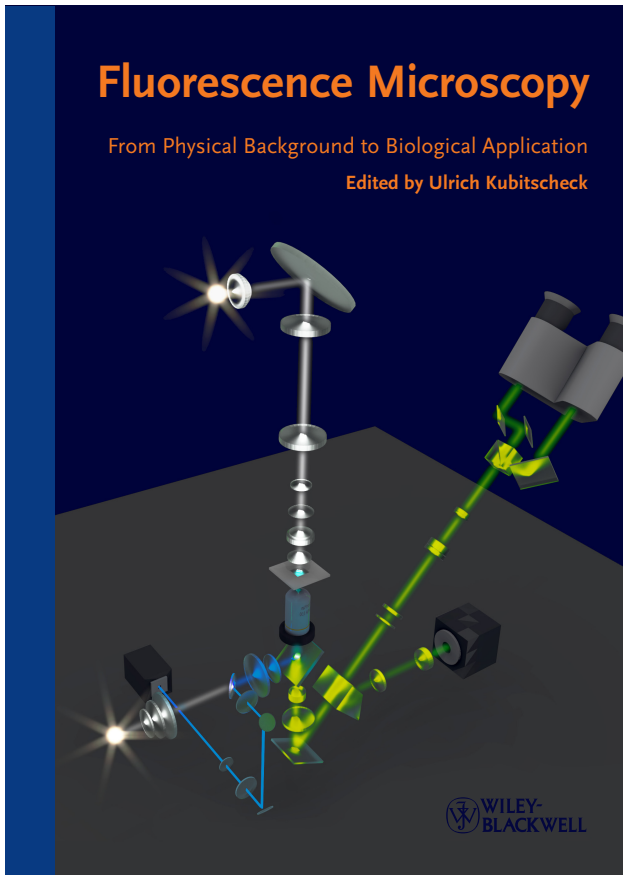

To be published in April 2013

Acknowledgements

Biophysical chemistry group, Bonn

Lisa Büttner c
Eugen Baumgart p
Tim Kaminski b
Florian Kotzur c
Xinliang Liu b
Claudio Nietzel t
Maximilian Schiener c
Dr. Karl Schmitz c
Katharina Scherer c
Ulrike Schmitz-Ziffels c
Dr. Jan-Peter Siebrasse b
Jan-Hendrik Spille p
Andreas Veenendaal p

Former group members

Johannes Anzt c
Sarah Benter c
Claus Bier c
Dr. Corina Ciobanasu c
Sandra Cordes c
Thomas Dange b
Prof. Dr. David Grünwald bp
Enno Harms c
Dr. Andreas Hoekstra p
Constanze Husche c
Dr. Birgit Klaiberg c
Oliver Kückmann p
Dr. Thorsten Kues p
Dr. Jörg Ritter p
Dr. Daniel Rohleder p
Dr. Jasmin Speil b
Dr. Beatrice Spottke c
Dr. Roman Veith b
Werner Wendler t

Karolinska Institutet, Stockholm, Sweden
Prof. Dr. Bertil Daneholt
Goethe University of Frankfurt, Germany
Prof. Dr. Alexander Heckel
LaVision BioTec, Bielefeld, Germany
Dr. Heinrich Spiecker, Volker Andresen

Funding by BMWi, DFG, EU and Bonn University is gratefully acknowledged